Measurement and compensation of combined resonance driving terms in SESRI

Cheng Guo,[1,2] Jie Liu,[1,2] and Jian-Cheng Yang[1,2,*]

[1]*Institute of Modern Physics, Chinese Academy of Sciences, Chinese Academy of Sciences, Lanzhou 730000, China*

[2]*University of Chinese Academy of Sciences, Beijing 100049, China*

In high-intensity synchrotrons, usually with strong effect of nonlinearity, like the High Intensity heavy-ion Accelerator Facility (HIAF), the inevitable large incoherent space-charge-induced tune spread will cross resonance lines, leading to beam instability. As a result, the space charge resonance compensation scheme becomes a vital technology for achieving high intensity. In this paper, the feasibility of resonance compensation and the stabilization of particles extremely close to the resonance line, $Q_x = \frac{5}{3}$, are demonstrated in the experiments conducted at the Space Environment Simulation and Research Infrastructure (SESRI) synchrotron. A study on Resonance Driving Terms (RDTs) applied to SESRI is conducted with a particular focus on the Combined RDTs (CRDTs). A linear relevance between the strength of sextupole correctors and CRDTs was experimentally established, through which the effective resonance compensation was finally achieved. Furthermore, the issue of frequency leakage was mitigated by introducing a new simple method. Although limited by corrector precision, this work shows a great compensation effect in SESRI. Meanwhile, this study confirms the stabilization of particles extremely close to the resonance line. It is the foundation for space charge resonance compensation scheme in the HIAF, as well as in other high-intensity synchrotrons. In these high-intensity synchrotrons, the tune spread is limited by the resonance lines, because particles that cross resonance lines will lose under the resonance caused by the combined effect of space charge resonance crossing and magnet errors. In order to break through this limitation, the space charge resonance compensation scheme is our subsequent target.

Keywords: SESRI, Nonlinearity, Resonance compensation, Frequency leakage

I. INTRODUCTION

In synchrotrons, achieving accurate magnetic fields are essential. However, imperfections of the magnetic fields could result from many inevitable factors, including but not limited to manufacturing imperfections, alignment errors, fluctuations in power supply, eddy currents [1], hysteresis effects. These imperfections could induce nonlinearity and lead to non-structure resonances, which diminishes beam lifetime, reduces dynamic aperture, and increases beam loss. The compensation for these magnetic field errors plays a significant role in accelerator physics research.

In this paper, two experiments were conducted at the Space Environment Simulation and Research Infrastructure (SESRI) synchrotron [2], constructed by the Institute of Modern Physics and located at the Harbin Institute of Technology. These experiments are performed near the resonance line, $Q_x = \frac{5}{3}$, with over 90% beam loss when deactivating sextupole correctors. In this work, a notable resonance compensation effect was achieved, experimentally demonstrating that particles could remain stable in the vicinity of 3rd-order resonance lines under appropriate compensation. The primary aim of these experiments was to experimentally verify the resonance compensation scheme by measuring and minimizing the Resonance Driving Terms (RDTs) and to perform preliminary research for the High Intensity heavy-ion Accelerator Facility (HIAF) [3].

The nonlinear beam dynamics is still a big challenge for high-quality beam. The study on the effects of systematic coupling resonances [4], the slow extraction [5], and the design of a proton therapy system [6–8] shows the importance of the nonlinearity in accelerator physics. RDTs are useful tools for studying the nonlinear effects of magnetic fields on particle beams in synchrotrons [9]. It focuses on identifying and quantifying the effects of specific perturbations that could induce resonant behavior of the beam. The Hamiltonian of the system could be expressed as a series of Fourier coefficients that depend on the amplitude and phase of the beam oscillations [10]. RDTs have been applied in various experiments, including the measurement of the linear coupling, the sextupole RDTs, and the octupole RDTs at different energies and intensities in the CERN Super Proton Synchrotron (SPS) [11]. RDTs were measured in order to validate the nonlinear optics commissioning [12] and realize the chromatic coupling correction [13] of the Large Hadron Collider (LHC). In the experiment conducted at the BNL Relativistic Heavy Ion Collider (RHIC), the Three Beam Position Monitors (BPMs [14–16]) method, which is derived from RDTs, was utilized to measure the global and local resonance terms [17]. At the European Synchrotron Radiation Facility (ESRF), the Combined RDTs (CRDTs) method, which requires only one BPM for the measurement and correction of nonlinearity in the synchrotron, was also confirmed through the application of RDTs [18]. Additionally, RDTs also play an important role in analyzing resonances excited by the space charge potential in synchrotrons [19]. More theoretical research of RDTs can be found in [20].

RDTs need harmonic analysis of data from BPMs to identify the spectral components associated with different multipole fields. To record the particle oscillation data, a Turn-by-Turn (TbT) acquisition system is required. This system could capture the beam position information during the oscillations and, after normalizing this position information, Fourier analysis could extract individual spectral components required for

* Corresponding author, yangjch@impcas.ac.cn

RDTs. The development of TbT acquisition systems dates back to the 1990s [21].

How to realize the stabilization of particles crossing resonance lines is a vital issue for high-intensity synchrotrons like HIAF, beacuse of the large tune spread, $\triangle\nu_x \approx -0.23$, $\triangle\nu_y \approx -0.37$, due to space charge effect [22]. Beam instability due to the inevitable resonance crossing is the main limitation. In this paper, the stabilization of particles extremely close to $Q_x = \frac{5}{3}$ was realized through the resonance compensation scheme described in In Sec. III D.

The paper is structured as follows. In Sec. II, theoretical derivations and simulation work of the compensation scheme employed in the experiments is conducted. In Sec. III, the progress, result and analysis of the two experiments is shown, including the raw data acquisition, the frequency leakage issue, compensation scheme, and the results of the two experiments. Sec. IV contains a summary of the whole paper.

II. FORMALISM AND SIMULATION

A. CRDTs Formalism

The Formalism of RDTs, a theoretical framework on nonlinear beam dynamics, is based on the description in normal forms of the beam oscillations as shown in Eq. (1). According to RDTs, the horizontal TbT data of the complex Courant-Snyder variables at the location of the BPM, denoted as b, can be decomposed into a series of Fourier components [18]:

$$\begin{aligned}[\widehat{x} - i\widehat{p}_x](N,b) =& \sqrt{2I_x}e^{i(2\pi\nu_x N+\phi_{x_b})} \\ &- 2i\sum_{jklm} j f^{(b)}_{jklm}(2I_x)^{\frac{j+k-1}{2}}(2I_y)^{\frac{l+m}{2}} \\ &\times e^{i[(1-j+k)(2\pi\nu_x N+\phi_{x_b})+(m-l)(2\pi\nu_y N+\phi_{y_b})]}\end{aligned} \tag{1}$$

where $\widehat{x}$ and $\widehat{p}_x$ are the normalized coordinates, $I_{x,y}$ and $\phi_{x,y}$ are the nonlinear action-angle variables, and $\nu_{x,y}$ are the tunes influenced by detuning due to either linear coupling or amplitude dependent effects. The horizontal and vertical phases of the lattice at the BPM location b are denoted as ϕ_{x_b,y_b}. According to Eq. (1), the fundamental tune line ν_x and numerous secondary lines, such as $(1-j+k)\nu_x + (m-l)\nu_y$, generated by corresponding nonlinear magnets, will arise within the spectrum of $\widehat{x} - i\widehat{p}_x$.

The resonance driving terms in Eq. (1), f_{jklm}, are :

$$f^{(b)}_{jklm} = \frac{\sum_\omega h_{\omega,jklm}e^{i[(j-k)\triangle\phi^b_{\omega,x}+(l-m)\triangle\phi^b_{\omega,y}]}}{1-e^{2\pi i[(j-k)Q_x+(l-m)Q_y]}} \tag{2}$$

where the ω is the location of the ω^{th} multipole, the $\triangle\phi^b_{\omega,x,y}$ is the phase advance between the ω^{th} multipole and the location b, and the $h_{\omega,jklm}$ is:

$$\begin{aligned}h_{\omega,jklm} &= -\frac{\Omega_{\omega,n-1}(l+m)}{j!k!l!m!2^{j+k+l+m}} i^{l+m}(\beta_{\omega,x})^{\frac{j+k}{2}}(\beta_{\omega,y})^{\frac{l+m}{2}} \\ \Omega_{\omega,n-1}(l+m) &= \begin{cases} K_{\omega,n-1}L & \text{if (l+m) is even} \\ iJ_{\omega,n-1}L & \text{if (l+m) is odd} \end{cases}\end{aligned} \tag{3}$$

where n is the order of resonance, $n = j+k+l+m$, K is the normal multipole coefficient, J is the skew multipole coefficient and L is the length of the ω^{th} multipole. For example, when $jklm = 3000$, $\Omega_{\omega,n-1} = K2_\omega L$, and when $jklm = 0030$, $\Omega_{\omega,n-1} = iK2S_\omega L$.

According to Eq. (2), f_{jklm} will diverge when :

$$(j-k)Q_x + (l-m)Q_y = \ell \tag{4}$$

where the ℓ is any integer. When Eq. (4) is satisfied, resonances occur. Besides, the most important value of $jklm$ could be identified through Eq. (4). For example, when $Q_x = 1.67$, which means that $(3-0)Q_x + (0-0)Q_y \approx 5$, attention should be paid to the situation $jklm = 3000$. Substitute $jklm = 3000$ into Eq. (1) and ignore other f_{jklm}, it is obvious that the tune line, ν_x, and the secondary line driven by the sextupole fields, $-2\nu_x$, in the horizontal spectrum should be of concern.

Returning to Eq. (1), $\widehat{x}$ could be determined by using the TbT acquisition system, while the reconstruction of $\widehat{p}_x$ is achieved by using data from two BPMs [21]. Fourier analysis of $\widehat{x} - i\widehat{p}_x$ could extract information about the coefficients f_{jklm}, crucial for resonance measurement and compensation. Unfortunately, successful $\widehat{p}_x$ reconstruction needs a region where there is no nonlinearities between the two synchronized BPMs. In the SESRI synchrotron, such region does not exist because there are dipoles with nonlinearity between any two horizontal or vertical BPMs. However, the measurement of CRDTs remains possible even without $\widehat{p}_x$ information.

CRDTs are linear combinations of RDTs, aiming to analyze the real part of $\widehat{x} - i\widehat{p}_x$. As previously discussed, with $Q_x = 1.67$, the $-2\nu_x$ spectral line in $\widehat{x} - i\widehat{p}_x$ is influenced by the coefficient f_{3000}. However, the $-2\nu_x$ spectral line in $\widehat{x}$ is composed of both the $+2\nu_x$ and $-2\nu_x$ spectral lines from $\widehat{x} - i\widehat{p}_x$. This implies that this CRDT includes not only f_{3000} at the $-2\nu_x$ line but also f_{1200} at the $+2\nu_x$ line. A simple derivation can be found in equations D15-D17 of arxiv version of [18]:

$$\begin{aligned}\widehat{x}(N,b) =& \frac{\sqrt{2I_x}}{2}[e^{i(2\pi\nu_x N+\phi_{x_b})} + e^{-i(2\pi\nu_x N+\phi_{x_b})}] \\ &- 2iI_x(3f^{(b)}_{3000} - f^{(b)*}_{1200})e^{-i2(2\pi\nu_x N+\phi_{x_b})} \\ &+ 2iI_x(3f^{(b)*}_{3000} - f^{(b)}_{1200})e^{i2(2\pi\nu_x N+\phi_{x_b})}\end{aligned} \tag{5}$$

from which the CRDT corresponding to f_{3000} is:

$$F^{(b)}_{NS3} = 3f^{(b)}_{3000} - f^{(b)*}_{1200} \tag{6}$$

According to Eq. (2,3), Eq. (6) can be rewritten as:

$$F^{(b)}_{NS3} = \sum_\omega 3h_{\omega,3000}[\frac{e^{i3\triangle\phi^b_{\omega,x}}}{1-e^{i6\pi Q_x}} - \frac{e^{i\triangle\phi^b_{\omega,x}}}{1-e^{i2\pi Q_x}}] \tag{7}$$

with $h_{\omega,1200} = 3h_{\omega,3000}$. Two key conclusions can be drawn from Eq. (7). Firstly, $F^{(b)}_{NS3}$ has a linear relevance with each sextupole magnetic field within the synchrotron. Secondly, under conditions where the tune satisfies $3Q_x \approx$ N

($Q_x \neq$ N), in most cases when errors are randomly distributed in the synchrotron, the amplitude of $f^{(b)}_{3000}$ greatly exceeds that of $f^{(b)}_{1200}$, achieving the approximation $F^{(b)}_{NS3} \approx 3f^{(b)}_{3000}$. However, it is important to note that this approximation might be broken when $\left|\sum_\omega h_{\omega,3000} e^{i3\triangle\phi^{(b)}_{\omega,x}}\right| \approx 0$ or $\left|\sum_\omega h_{\omega,3000} e^{i\triangle\phi^{(b)}_{\omega,x}}\right|$ is too big. For example, in the realm of linear coupling, it was observed that $|f_{1001}|$ exceed $|f_{1010}|$, even though the tune was closer to the difference resonance (1,-1) excited by f_{1001} than to the sum resonance (1,1) excited by f_{1010} in the ESRF [23].

To summarize, although only $\widehat{x}$ is measurable, it is possible to set the tune into the vicinity of $3Q_x \approx$ N condition to achieve $F^{(b)}_{NS3} \approx 3f^{(b)}_{3000}$. Then, the linear relevance between $F^{(b)}_{NS3}$ and the intensity of each sextupole magnet could be measured. As a result, the measured linear relevance between $F^{(b)}_{NS3}$ and the strength of sextupole correctors could be effectively used in compensation for sextupole field errors with even only one BPM, resulting in similar effects with compensation scheme through $f^{(b)}_{3000}$. It is important to add that the the general compensation scheme aims to match and minimize (C)RDTs all along the ring [24], which means that usually (C)RDTs at all BPMs should be measured and minimized. But in later experiments, the sextupole fields in the ring only arises from the alignment errors, high-order magnetic field errors of dipoles and quadrupoles, and the hysteresis of sextupoles, which means that there are no strong sextupole fields, causing that the amplitude of $f^{(b)}_{3000}$ keeps almost the same all along the ring. As a result, the compensation scheme with only one BPM introduced by this paper can be effective in this situation, but it might not realize the optimal compensation when strong sextupole fields, like chromaticity sextupoles, were activated.

In conclusion, the key idea of this section is to realize the approximation $F^{(b)}_{NS3} \approx 3f^{(b)}_{3000}$ when $3Q_x \approx$ N through Eq. (7), in order to make the measurement and compensation capable with even one BPM. Besides, as the whole scheme is under the condition of $3Q_x \approx$ N, the amplitude of secondary lines driven by sextupoles in the horizontal spectrum should be large enough to be measured by BPMs.

B. Simulation

The idea was tested by using MADX-PTC single particle tracking [25, 26], within the ideal lattice model of SESRI synchrotron. To induce resonance, a small sextupole magnet was introduced into the lattice, while maintaining the tune at $Q_x = 1.67, Q_y = 1.74$. The spectrum of beam oscillation, as depicted in Fig. (1), provides the information for the calculation of $f^{(b)}_{jklm}$ and $F^{(b)}_{NS3}$ values: $3f^{(b)}_{3000} = -1.840 - 3.265i$, $f^{(b)}_{1200} = -0.015 + 0.082i$, and $F^{(b)}_{NS3} = -1.825 - 3.183i$. Through adjusting the sextupole magnet and analyzing the spectrum of $\widehat{x} - i\widehat{p}_x$ and $\widehat{x}$, two clear linear relevances are shown in Fig. (2). Through the measurement of the relevance between $K_{\omega,2}L$ and both $F^{(b)}_{NS3}$ and $f^{(b)}_{3000}$, the two conclusions drawn earlier are confirmed: (1) $F^{(b)}_{NS3}$ displays a linear dependence on the sextupole strength, and (2) when the tune satisfies $3Q_x \approx$ N, $F^{(b)}_{NS3} \approx 3f^{(b)}_{3000}$. As a result, when $3Q_x \approx$ N, it is feasible to reduce the amplitude of $F^{(b)}_{NS3}$ by taking advantage of its linear relevance with the sextupole field and making corresponding adjustments to sextupole correctors. This approach would ultimately reduce the amplitude of $f^{(b)}_{3000}$, making the beam oscillation stable and mitigating the resonance.

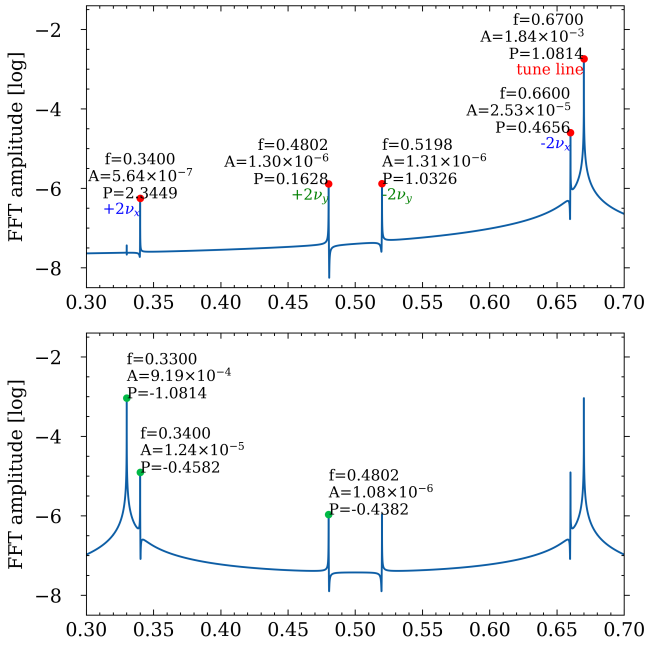

Fig. 1. The spectrum of $\widehat{x} - i\widehat{p}_x$ (top) shows the fundamental tune line ν_x and other 4 secondary lines, -2ν_x for f_{3000}, +2ν_x for f_{1200}, and $\pm 2\nu_y$ for f_{1020} and f_{1002}, all driven by normal sextupole. In the spectrum of $\widehat{x}$ (bottom), the [0.5,1] part is complex conjuage of [0,0.5], where the information of lines can be found in Eq. (5).

In conclusion, as the two key conclusions described in Sec.II A has been confirmed by the simulation, the compensation scheme in the subsequent experiments could be designed as follows. Step 1, acquire reliable beam oscillation data through the TbT acquisition system while setting the tune as close as possible to $Q_x = \frac{5}{3}$. To get such TbT data, an excitation, like kickers or RF-knockout (RF-KO) [27, 28], should be introduced in the progress of the data acquisition while avoiding too much beam loss in order to ensure the precision of the TbT data. Step 2, deal with the TbT data through Fourier analysis, and check corresponding lines in the spectrum, then calculate the value of $F^{(b)}_{NS3}$ by using the information of these lines. Step 3, repeat the measurement and calculation for a few times to get the average and standard deviation. Step 4, adjust the strength of the sextupole corrector and get back to step 3 until the linear relevances are obtained. Step 5, calculate the compensation through the linear relevances and detect the beam intensity to check the effect of the compensation.

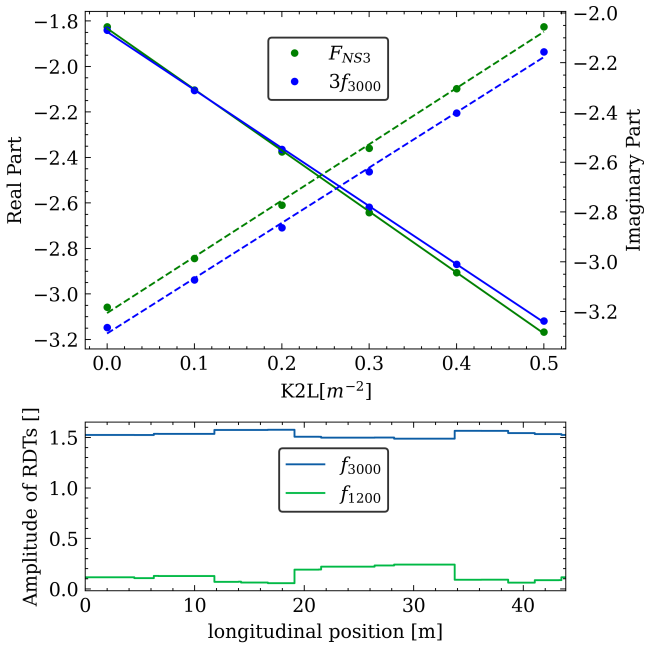

Fig. 2. The top figure shows that, by changing the value of $K2L$, the variation of $F^{(b)}_{NS3}$ and $3f^{(b)}_{3000}$ is observable. Solid lines show the real part, which are almost overlapping, while dotted lines represent the imaginary part. The bottom figure shows the amplitude of f_{3000} and f_{1200} all along the ring.

C. Discussion On The Systematic Resonance

Nonlinear resonances are classified into systematic and random resonances. Systematic nonlinear resonances are located at $\ell = \mathrm{P} \times integer$, where P is the superperiod of an accelerator [29]. A systematic resonance may be hit even without magnet errors. If a systematic resonance happened at $Q_x = \frac{5}{3}$, it would be impossible to realize the beam compensation just by sextupole correctors. The analysis of systematic resonance in the SESRI lattice is shown in Fig. (3). As the analysis shows, the two closest resonance lines, $3Q_x = 5$ and $4Q_y = 7$, do not satisfy the condition $\ell = 6 \times integer$, which means the systematic resonances would not happen at the target configuration.

III. EXPERIMENT

A. Parameter Setting

$^{209}Bi^{32+}$ at 7.03 MeV/nucleon was used in experiments of this paper. The radio frequency (RF [30, 31]) cavity kept switching on during the whole ramping in order to make sure the beam was single bunch at the period of measurement. The RF-KO switched on with constant amplitude and single frequency for 0.004s, equal to about 3400 turns, at the extraction-platform to excite the beam oscillation.

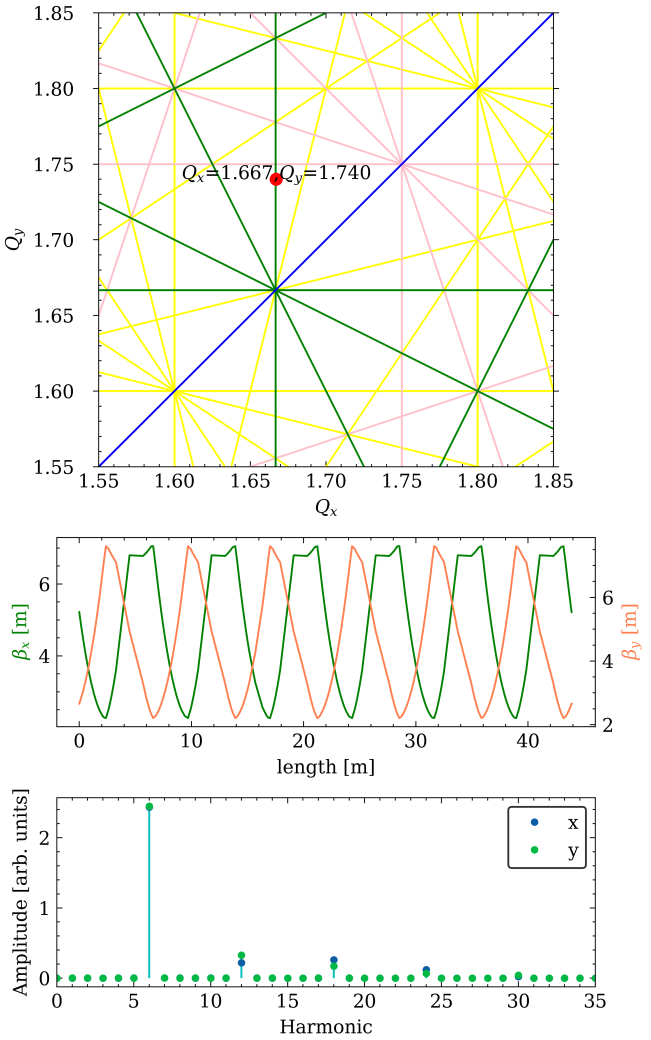

Fig. 3. The top figure shows the tune diagram of the target configuration with up-to 5th order resonance lines. The middle figure shows the β_x and β_y function and the bottom figure shows the harmonic analysis of the β function.

B. Data Acquisition

In the experiments, when $Q_x > \frac{5}{3}$, it was observed that when the tune configuration got lower than $Q_x = 1.676$, the decay of free beam oscillation became excessively rapid, making it challenging to acquire reliable TbT data. So, the final tune during measurement was set to $Q_x = 1.676$. An example of the raw TbT data measured at the SESRI synchrotron is shown in Fig. (4), with the maximum length of the TbT data being 65536.

The subsequent step involves analyzing the spectrum using Fast Fourier Transform (FFT). FFT is a common algorithm for Fourier analysis, capable of transforming a signal from its time or space domain into the frequency domain. The key factors of FFT analysis include the signal's length, noise levels, sampling rate, window function. For the data acquired via the TbT system, the sampling rate corresponds to the cyclotron

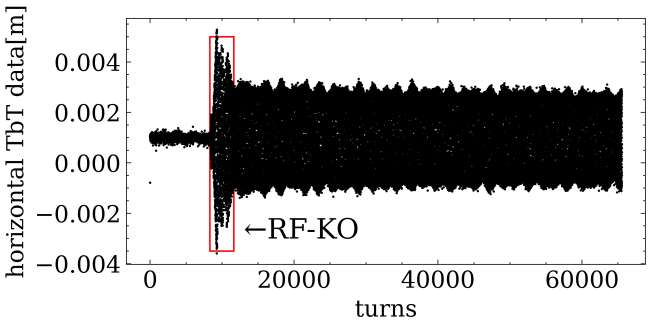

Fig. 4. An example of raw TbT data measured at the SESRI synchrotron. Slow-extraction excitation RF-KO, which would last for about 3400 turns, is used to excite the beam.

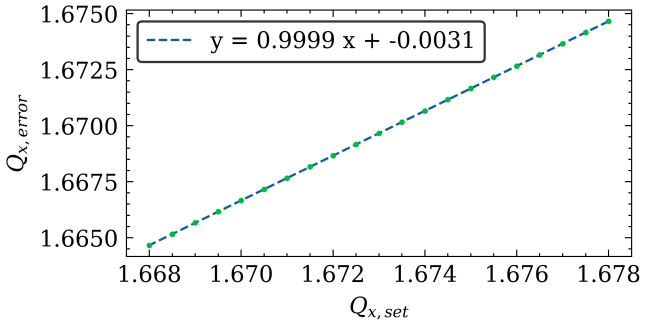

Fig. 6. Quadrupole errors are introduced into the lattice by EFCOMP order of MAD-X, causing the difference in $Q_{x,set}$ and $Q_{x,error}$. $Q_{x,set} - Q_{x,error} \approx 0.0031$ is observed by changing $Q_{x,set}$ while keep random seed unchanged. By changing the seed, the gradient would vary from 0.98 to 1.02. In conclusion, $Q_{x,set} - Q_{x,real} \approx 0.0031$ is not a strict relevance, but an approximation to infer $Q_{x,real}$ when $Q_{x,real}$ is unmeasurable due to strong nonlinearity in the vicinity of the $Q_x = \frac{5}{3}$.

frequency of the synchrotron, and the window function was not used in this paper. As a result, the primary factors affecting the FFT results are the available TbT data length and the data noise.

Fig. (5) illustrates an example of the FFT result with data positions from 20,000 to 36,383 turns. Several conclusions can be made from the figure: (1) The noise of the TbT data is approximately within the range of $\pm 1\mu m$. This precision is good enough since the line $-2\nu_x = 0.3456$ would not be observable if the noise exceeded $\pm 10\mu m$. (2) The actual tune is $Q_{x,real} = 1.6729$, while the value set on the user interface is $Q_{x,set} = 1.676$, indicating that the experiments are under the condition of $Q_{x,set} - Q_{x,real} \approx 0.0031$, which could be proven by a simulation in Fig. (6).

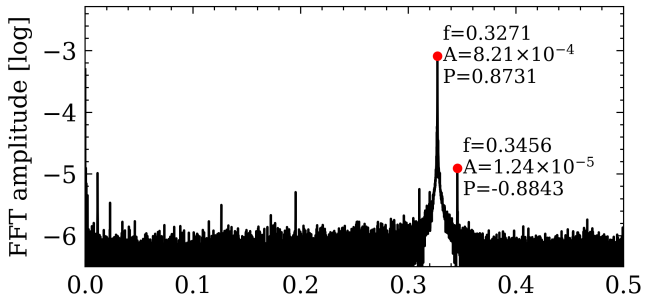

Fig. 5. An example of the FFT result from 20000 to 36383 turns. The measured value of $k \times F^{(b)}_{NS3}$ differs from $F^{(b)}_{NS3}$ without considering the normalization of x and the BPM calibration factor. The measured value through this graph is $3.498 + 3.000i$.

It is important to note that the FFT result in Fig. (5) is based on the raw x, rather than the normalized $\widehat{x}$, due to the incomplete measurement of β_x. Furthermore, using the BPM calibration factor alone would be meaningless, so the calibration factor has not been taken into account. Obviously, calculated results from raw x, without considering β_x and BPM calibration factor, are not $F^{(b)}_{NS3}$. To maintain rigor in our analysis, it is essential to introduce a new quantity, denoted as $k \times F^{(b)}_{NS3}$, where k is a dimensionless non-zero real number. k serves as a scaling factor between the values obtained from our spectrum calculations and the actual value of $F^{(b)}_{NS3}$. However, even without the precise value of k, the linear relevance could still be measured, resulting in the same compensation configuration. Therefore, the compensation for sextupole field errors could be done just by experimentally measuring the linear relevance between $k \times F^{(b)}_{NS3}$ and the strength of the sextupole correctors, and adjusting the sextupole correctors. Stubbornness in the actual value of $F^{(b)}_{NS3}$ would only make the compensation scheme more complicated.

C. Frequency Leakage Issue

At first, $2^{14} = 16384$ was chosen as the length of FFT. When the data length is a power of 2, the FFT algorithm achieves its lowest computational complexity. As a result, a power of 2 is usually chosen as the FFT data length. However, in fact, FFT, like scipy.fftpack.fft used in this paper, could handle any data length.

In order to fully utilize the TbT data, the FFT starting turn number was incrementally adjusted from 20000 to 40000, while maintaining a constant FFT data length of 16384. The amplitudes and phases of all $k \times F^{(b)}_{NS3}$ were visualized in Fig. (7). From the figure, two significant conclusions were made: (1) the amplitude variation reached ± 0.7, corresponding to a large error of $\pm 18\%$. (2) The phase exhibits an oscillatory behavior, alternating between two values differing by about π.

It was eventually determined that the observed strange phenomena was derived from the frequency leakage issue. Frequency leakage refers to the undesired phenomenon in which a signal or frequency component unintentionally leaks into adjacent frequency grids. This issue is commonly a result of imperfections in signal processing systems. Such imperfections could lead to the unintended bleeding of energy from the target frequency line into neighboring frequency grids.

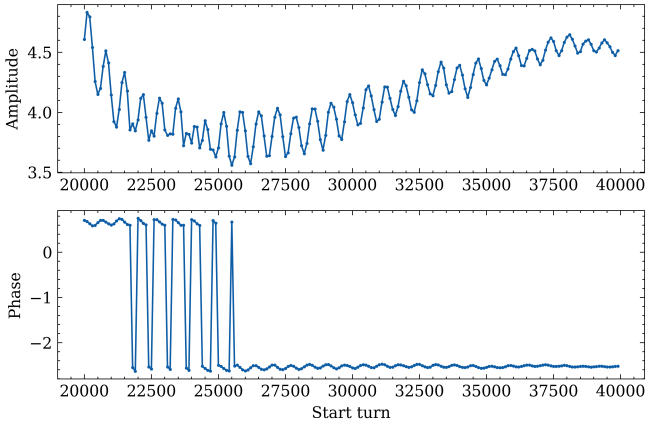

Fig. 7. The FFT starting turn number was incrementally adjusted from 20000 to 40000, while maintaining a constant FFT data length of 16384. The amplitudes and phases of every $k \times F_{NS3}^{(b)}$ were recorded. Based on the strange phase discontinuity phenomenon observed in the bottom figure, it could be inferred that there may be an issue with the data processing methodology.

To visually show the impact of the frequency leakage issue in our experiment, a comparison was made between the spectra with FFT starting points at 21900 and 22000 turns. The spectra were analyzed, and the last points of key lines were marked in green, while the next points were marked in blue, as shown in Fig. (8). The data used for the two figures differed only by a 100-turn FFT starting point interval. This implies that the two segments were almost the same. However, the calculated values of $k \times F_{NS3}^{(b)}$ for the two figures were $-3.357 - 1.7.6i$ and $2.874 + 2.690i$ respectively, indicating a phase difference of 3.384. It is evident that serious frequency leakage has occurred in the sextupole-driven lines in both figures, making the calculated results unreliable. Therefore, sloving the issue of frequency leakage is vital to obtain accurate results.

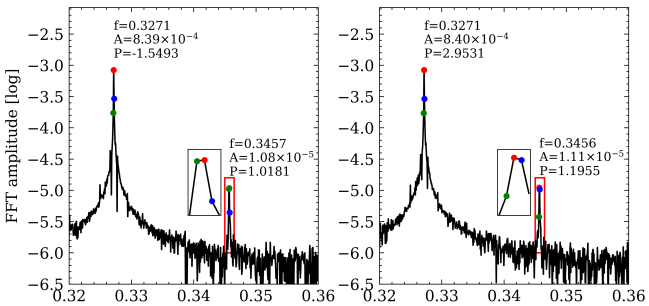

Fig. 8. A comparison between the spectrum with FFT starting points at 21900 (left) and 22000 (right), both with a constant FFT data length of 16384. The calculated values of $k \times F_{NS3}^{(b)}$ are $-3.357 - 1.7.6i$ and $2.874 + 2.690i$ respectively, indicating a phase difference. The last points of vital lines are marked in green, while the next points are marked in blue. The red box parts are magnified to show that frequency leakage has occurred in the sextupole-driven lines in both figures.

Previous studies have introduced several mathematical methods aimed at mitigating frequency leakage [32]. However, these methods are effective only in cases where the frequency leakage is not severe. In situations where the amplitudes of key peaks and their neighboring points are nearly equal, as illustrated in Fig. (8), even the utilization of these mathematical approaches would not get accurate results.

This paper introduces a new method for mitigating the effects of frequency leakage: adjusting the FFT data length. This approach is based on the following principles: The accuracy of the frequency, amplitude, and phase in spectral analysis is based on the alignment of normalized frequency grids with specific spectral lines. When a normalized frequency grid aligns with the target frequency, the calculated values are precise. However, if the target frequency falls between two normalized frequency grids, the values of frequency and amplitude become less accurate, leading to errors.

For example, as shown in Fig. (9), an complex array of $Z(N) = e^{2\pi i \times 0.2N}$ is analyzed through FFT with data length 1024 (left) and 1025 (right) respectively. In the left figure, FFT with data length 1024 could not provide a normalized frequency grid aligning with 0.2, instead in the right figure, FFT with data length 1025 could provide a normalized frequency grid, $\frac{205}{1025}$, aligning with 0.2. As a result, in the left figure, the frequency, amplitude, and phase are all incorrect because the frequency leakage occurs.

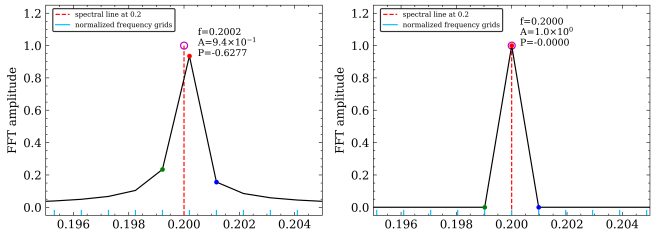

Fig. 9. An complex array of $Z(N) = e^{2\pi i \times 0.2N}$ is analyzed through FFT with data length 1024 (left) and 1025 (right) respectively. Compared to the data length 1025, FFT with data length 1024 could not provide a normalized frequency grid aligning with 0.2. As a result, the frequency leakage takes place and the frequency, amplitude, and phase are incorrect in the left figure.

In conclusion, to solve the issue of frequency leakage, an appropriate FFT data length could be chosen to ensure that normalized frequency grids align with both the fundamental line and the sextupole-driven line. For example, the degree of frequency leakage, denoted as FL, could be defined as follows:

$$FL_n = \left| \frac{A_{n-1} - A_{n+1}}{A_{n-1} + A_{n+1}} \right|, \tag{8}$$

where n represents the position of interest in the frequency domain, A_{n-1} is the amplitude of its last point, and A_{n+1} is that of its next point. It is important to note that the definition in Eq. (8) is for the sake of convenience in subsequent data processing, and it may not necessarily be the optimal approach. The choice of the appropriate definition should be

carefully considered based on the specific requirements of the analysis.

In order to mitigate frequency leakage in both the fundamental line and the sextupole-driven line, the relevance between the $FL_{n(\nu_x)} + FL_{n(-2\nu_x)}$ and the FFT data length is plotted in Fig. (10). The left figure represents the FFT starting point at 21900, while the right one shows the FFT starting point at 22000. This analysis helps identifying the optimal FFT data length that minimizes the frequency leakage at these specific spectral lines. In the top two plots of Fig.(10), the most suitable FFT data lengths were found within the range [16284, 16484], as the most small $FL_{n(\nu_x)}+FL_{n(-2\nu_x)}$ were achieved with lengths of 16438 and 16328, respectively. The corresponding data segments were used in Fourier analysis, producing the bottom two plots. The comparison between Fig.(8) and Fig.(10) reveals a significant reduction in the effects of frequency leakage at the spectral lines after applying this approach of adjusting the FFT data length. Utilizing the result from Fig.(10), calculations were performed for $k \times F^{(b)}_{NS3}$ values of $-3.916-2.646i$ and $-3.919-2.615i$. As a result, the large phase difference in Fig.(8) was eliminated.

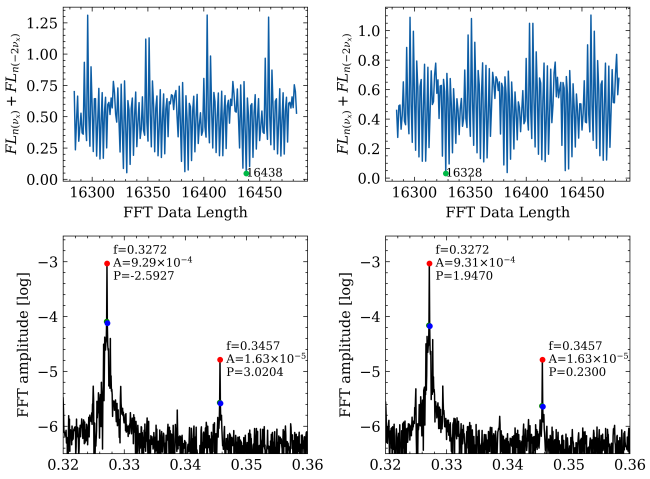

Fig. 10. The relevance between the degree of frequency leakage and the FFT data length (top 2 figures, the start point of left is 21900 and that of right is 22000), and FFT results with corresponding data segments (bottom 2 figures, the data segments of left is from 21900 to 28337 and that of right is from 22000 to 38327). The calculated values of $k \times F^{(b)}_{NS3}$ are $-3.916 - 2.646i$ and $-3.919 - 2.615i$ respectively. Compared with Fig. (8), the frequency leakage is reduced and the $k \times F^{(b)}_{NS3}$ values is more reliable.

By applying this method, Fig.(7) was reanalyzed to obtain Fig.(11). The reanalyzed figure illustrates a reduction in amplitude variation to ± 0.15, approximately $\pm 3\%$, while the phase remains stable at -2.54 ± 0.04. The phase oscillations previously observed in Fig. (7) have been eliminated.

In conclusion, the accuracy of frequency analysis could be improved by aligning normalized frequency grids with specific spectral lines through the adjustment to FFT data length, effectively reducing the impact of frequency leakage. The key point of this section is to introduce a new simple method by adjusting FFT data length to mitigate frequency leakage.

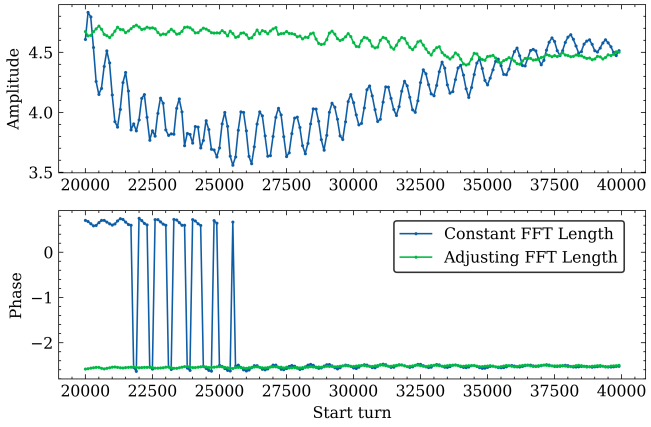

Fig. 11. After applying the approach of adjusting the FFT data length, Fig. (7) was reanalyzed. As a result, the error in amplitude is reduced, and the oscillatory behavior in phase has completely vanished.

D. Experiment results

In the first experiment, the huge error in amplitude and the strange discontinuity in phase were observed. However, the cause of these issues, frequency leakage, had not been realized at that time. These issues seriously influenced the precision of measured $k \times F^{(b)}_{NS3}$, resulting in an unreliable linear relevance with the strength of the sextupole correctors. The first compensation configuration calculated by this unreliable linear relevance made improvement in beam loss from 95% to 75%. But another attempt through manually scanning sextupole correctors in the vicinity of this configuration happened to realize a relatively good compensation. The results of the first experiment are showed in Fig. (12). The top figure shows a comparison of the intensity with and without compensation, shown on the DC current transformers (DCCT) [33] in the first experiment, with the extraction-platform's tune set at 1.673, while the actual tune was approximately 1.670. In the initial three ramping events, the sextupole correctors remained inactive, resulting in the beam loss of about 95%. Conversely, during the subsequent two ramping events, the sextupole correctors were activated, achieving the beam loss of approximately 25%, which was much less than that before compensation. Notably, shown in the bottom figure with the same configuration as the top figure, the effects of compensation were undergoing a dynamic change, with almost no beam loss in optimal results. This phenomena might be caused by power source instability, β beating and closed-orbit instability. According to the improvement of the beam performance with the compensation, it could be proved that the systematic resonance did not happen.

However, when the tune was set closer to $\frac{5}{3}$, the effect of the compensation configuration in the first experiment were rapidly reduced. For instance, when $Q_{x,real} \approx 1.667$, the beam loss still exceeded 90% even though activating compensation, indicating that complete compensation had not been attained. Consequently, after solving the frequency leakage

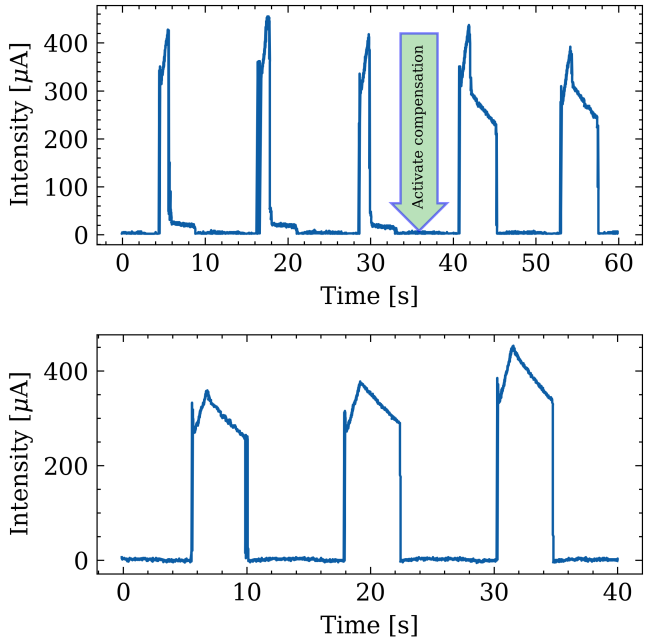

Fig. 12. Beam performance shown on DCCT when $Q_{x,real} \approx 1.670$ in the first compensation experiment. The first compensatory experiment showed the difference between the first three events of ramping without compensation and the subsequent two events of ramping with compensation (top). The effects of the compensation were undergoing a dynamic change, with almost no beam loss in optimal results (bottom).

issue, the second experiment commenced.

In the second experiment, the linear relevance between $k \times F^{(b)}_{NS3}$ and the strength of the sextupole correctors was finally established, as shown in Fig.(13). The experiment scheme, guided by the Sec. II, was as follows. Step 1, acquire reliable beam oscillation data like Fig. (4). Step 2, deal with the TbT data like Fig.(11) and obtain the value of $k \times F^{(b)}_{NS3}$. Step 3, repeat the measurement and calculation for 10 times to get the average and standard deviation. Step 4, adjust the strength of sextupole correctors, $K2(4S02)$ and $K2(4S04)$, then get back to step 3 until the satisfactory linear relevances are obtained. Step 5, calculate the compensation through the linear relevances and detect the beam intensity to check the effect of the compensation.

In Fig.(13), each data point in the figure corresponds to the average of 10 measurements carried out with the same $K2$ configuration. As shown in Fig.(11), the error of $k \times F^{(b)}_{NS3}$ from a single measurement is quite small. However, the error bars of 10 measurements remain relatively large. This phenomena could likely be attributed to a variety of factors, including but not limited to power supply instability, β beating, the instability of sextupole correctors itself. Nonetheless, the linearity composed by the averages is clear.

The SUSSIX was a program developed by Frank Schmidt and Riccardo Bartolini of CERN, in order to postprocess tracking or experimental turn-by-turn data via frequency analysis [34]. Fig. (14) is plotted by replacing Constant FFT Length in Fig. (11) with SUSSIX. The average amplitude and phase of SUSSIX and adjusting FFT length are almost the same. Furthermore, The 4S02 is used as an example to show the linear relevance comparison in Fig. (15). This comparison could show the reliability of our adjusting the FFT length method.

As mentioned before, the measurement of β function in the synchrotron had not been finished, making it incapable to attain the real lattice model. Still, the linear relevance obtained by the experiment was chosen as the basis of the compensation, which formulated into a response matrix R, resulting in $K2(4S02) \approx 1.678[m^{-3}]$ and $K2(4S04) \approx 0.387[m^{-3}]$.

$$\mathrm{R}\triangle\vec{k} + \overrightarrow{Error} = 0 \tag{9}$$

$$\begin{bmatrix} 1.962 & 0.520 \\ 1.080 & 1.857 \end{bmatrix} \begin{bmatrix} K2(4S02) \\ K2(4S04) \end{bmatrix} = \begin{bmatrix} 3.49 \\ 2.53 \end{bmatrix}$$

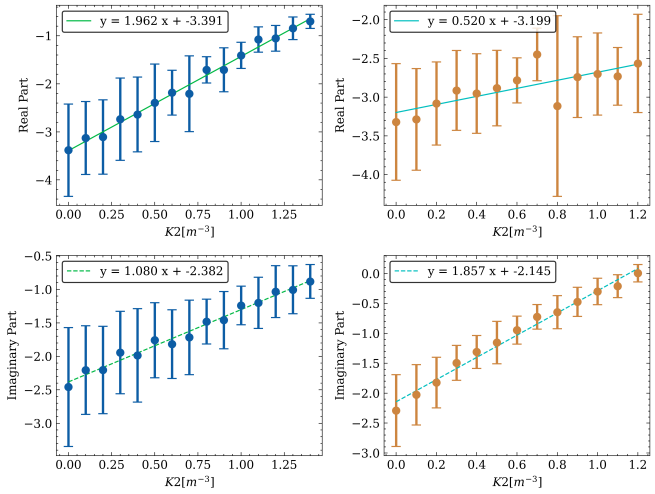

Fig. 13. The linear relevance between $k \times F^{(b)}_{NS3}$ and the strength of 2 series of sextupole correctors (left 2 figures are 4S02 and right 2 figures are 4S04). Acoording to the 4 linear functions in the figure, $K2(4S02) = 1.678[m^{-3}]$ and $K2(4S04) = 0.387[m^{-3}]$ were required to compensate for original sextupole errors in the SESRI synchrotron.

Finally, by applying the $K2$ of 4S02 and 4S04, and setting the tune at 1.670 (while the actual tune was approximately 1.667, the closest configuration to $\frac{5}{3}$), the screen captures of the DCCT are presented in Fig. (16). The observed beam loss varied from 10% to 50%, which was much better than that without compensation and that with compensation in the first experiment, indicating the strong resonance effect extremely close to the resonance line, where any tiny disturbance could lead to huge beam loss. The primary limitations of the compensation were the accuracy of the sextupole correctors and the overall stability of the synchrotron, because any manual adjustment by scanning the sextupole correctors did not make further improvements in the compensation.

In conclusion, by setting the tune as close as possible to $\frac{5}{3}$, the compensation method has proved successful. The key

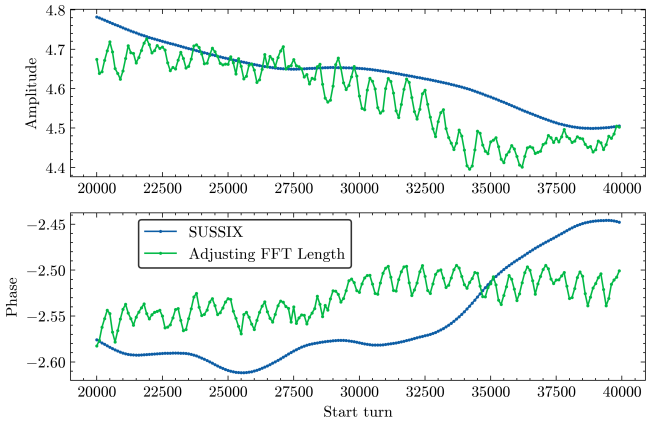

Fig. 14. The comparison between SUSSIX and adjusting FFT length in one turn-by-turn data file. The average amplitudes are respectively 4.63 and 4.57, and the average phases are respectively -2.55 and -2.53.

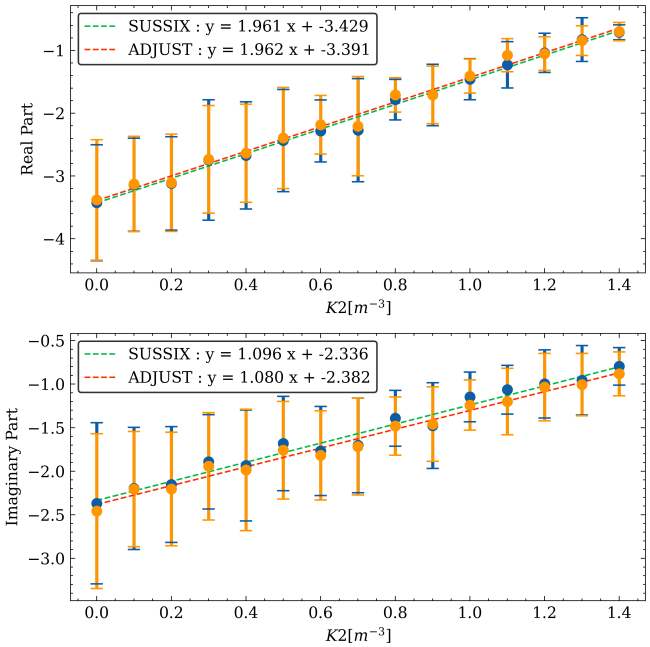

Fig. 15. The comparison between SUSSIX and adjusting FFT length in linear relevance of 4S02. The results are almost the same.

point of this section is to experimentally demonstrate that particles extremely close to the resonance line could remain stable with appropriate compensation.

IV. CONCLUSION

This article presents the resonance measurement and compensation extremely close to the resonance line, beginning with the establishment of important mathematical connections: (1) the linear relevance between $F_{NS3}^{(b)}$ and the sextupole field, and (2) the correlation of $F_{NS3}^{(b)}$ with $f_{3000}^{(b)}$ when

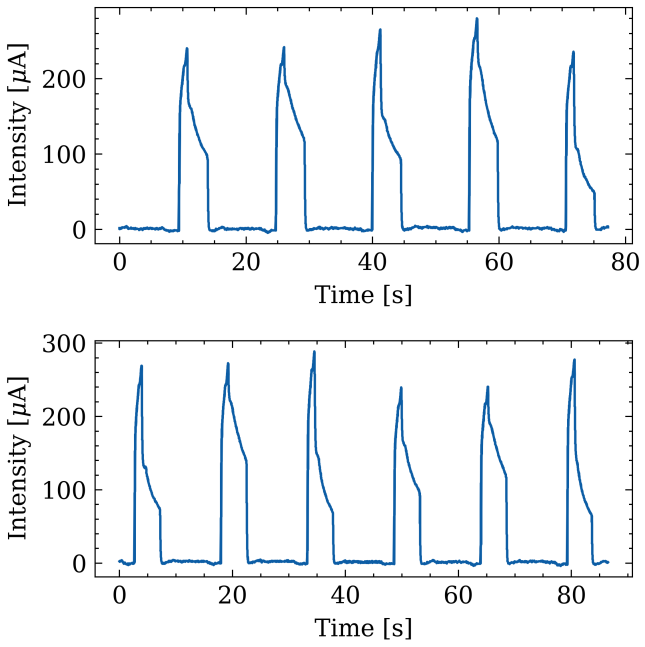

Fig. 16. Beam performance shown on DCCT when $Q_{x,real} \approx 1.667$ in the second compensation experiment.

the tune approaches $3Q_x \approx \mathrm{N}$. The MADX-PTC simulation was conducted to validate these ideas.

Subsequently, experiments of resonance measurement and compensation were conducted. The initial experiment faced the issue of frequency leakage, and successful results were achieved only at $Q_{x,real} \approx 1.670$, while the beam loss exceeded 90% at $Q_{x,real} \approx 1.667$. After analyzing a variety of factors, the frequency leakage issue was identified.

A new solution for frequency leakage issue was established in this experiment. It is to adjust the FFT data length to align normalized frequency grids with target spectral lines, which could reduce the frequency leakage. In the subsequent experiment, a linear relevance between $k \times F_{NS3}^{(b)}$ and the strength of sextupole correctors was successfully established. Despite it did not fit the ideal lattice model, it was chosen as the basis of the compensation.

Finally, under the condition of $Q_{x,real} \approx 1.667$, the compensation effect is significant. It was found that manual adjustments by scanning the correctors did not make any improvement. Therefore, it was concluded that the current compensation achieved in the SESRI synchrotron might be limited by the precision of the correctors and the compensation method had proved successful.

This article describes measuring the CRDTs with the tune extremely close to the resonance line, making it capable to achieve an effective resonance compensation. Through these experiments, it has been shown that the stabilization of particles extremely close to the resonance line could be maintained with appropriate compensation. This achievement sets a foundation for future work in resonance compensation at the High Intensity heavy-ion Accelerator Facility (HIAF), especially for particles under resonance crossing due to tune

spread. The research of space charge resonance compensation scheme in high intensity synchrotrons, which is the vital technology for overcoming the limitation of space charge effect, is our subsequent important work, with a a simulation code for high-intensity beams [].

V. ACKNOWLEDGEMENTS

This work was supported by the China National Funds for Distinguished Young Scientists (Grant No. 12425501).

[1] M.Z. Zhang, M. Zhang, X.C. Xie et al., Eddy current effects in a high field dipole. Nucl. Sci. Tech. **28**, 173 (2017). doi: 10.1007/s41365-017-0325-5

[2] S. Ruan, J.C. Yang, J.W. Xia et al., The 300 MeV proton and heavy ion accelerator complex for SESRI project in China. Nucl. Instrum. Meth. A. **1048**, 167916 (2023). doi: 10.1016/j.nima.2022.167916

[3] J.C. Yang, J.W. Xia, G.Q. Xiao et al., High intensity heavy ion accelerator facility (HIAF) in China. Nucl. Instrum. Meth. B. **317**, 263–265 (2013). doi: 10.1016/j.nimb.2013.08.046

[4] H.J. Zeng, S.Y. Lee, S.X. Zheng et al., Effects of systematic octupole coupling resonances. Nucl. Sci. Tech. **30**, 104 (2019). doi: 10.1007/s41365-019-0629-8

[5] Y.H. Yang, M.Z. Zhang, D.M. Li, Simulation study of slow extraction for the Shanghai Advanced Proton Therapy facility. Nucl. Sci. Tech. **28**, 120 (2017). doi: 10.1007/s41365-017-0273-0

[6] B. Qin, X. Liu, Q.S. Chen et al., Design and development of the beamline for a proton therapy system. Nucl. Sci. Tech. 32, 138 (2021). doi: 10.1007/s41365-021-00975-y

[7] M.Z. Zhang, D.M. Li, L.R.Shen et al., SAPT: a synchrotron-based proton therapy facility in Shanghai. Nucl. Sci. Tech. **34**, 148 (2023). doi: 10.1007/s41365-023-01293-1

[8] Y.H. Yang, M.Z. Zhang, D.M. Li, Simulation study of slow extraction for the Shanghai Advanced Proton Therapy facility. Nucl. Sci. Tech. **28**, 120 (2017). doi: 10.1007/s41365-017-0273-0

[9] G. Guignard, A general treatment of resonances in accelerators (1978). CERN. Report. doi: 10.5170/CERN-1978-011

[10] A. Bazzani, P. Mazzanti, G. Servizi et al., Normal forms for hamiltonian maps and nonlinear effects in a particle accelerator. Nuov. Cim. B. **102**(1), 51–80 (1988). doi: 10.1007/BF02728793

[11] R. Tomás, Direct measurement of resonance driving terms in the super proton synchrotron (SPS) of CERN using beam position monitors. CERN. Report. https://cds.cern.ch/record/615164

[12] E.H. Maclean, R. Tomás, F.S. Carlier et al., New approach to LHC optics commissioning for the nonlinear era. Phys. Rev. Accel. Beams. **22**(6), 061004 (2019). doi: 10.1103/PhysRevAccelBeams.22.061004

[13] T.H.B. Persson, Y.I. Levinsen, R. Tomás et al., Chromatic coupling correction in the large hadron collider. Phys. Rev. Spec. Top-AC. **16**(8), 081003 (2013). doi: 10.1103/PhysRevSTAB.16.081003

[14] J. He, Y.F. Sui, Y. Li et al., Design and fabrication of button-style beam position monitors for the HEPS synchrotron light facility. Nucl. Sci. Tech. **33**, 141 (2022). doi: 10.1007/s41365-022-01126-7

[15] J. He, Y.F. Sui, Y. Li et al., Beam position monitor design for the high energy photon source. Meas. Sci. Technol. **33**, 115106 (2022). doi: 10.1088/1361-6501/ac8277

[16] X.Y. Liu, F.F. Wu, T.Y. Zhou et al., Design and offline testing of a resonant stripline beam position monitor for the IR-FEL project at NSRL. Nucl. Sci. Tech. **31**, 70 (2020). doi: 10.1007/s41365-020-00778-7

[17] R. Tomás, M. Bai, R. Calaga et al., Measurement of global and local resonance terms. Phys. Rev. Spec. Top-AC. **8**, 024001 (2005). doi: 10.1103/PhysRevSTAB.8.024001

[18] A. Franchi, L. Farvacque, F. Ewald et al., First simultaneous measurement of sextupolar and octupolar resonance driving terms in a circular accelerator from turn-by-turn beam position monitor data. Phys. Rev. Spec. Top-AC. **17**(7) (2014). doi: 10.1103/PhysRevSTAB.17.074001

[19] F. Asvesta, H. Bartosik, Resonance Driving Terms From Space Charge Potential. CERN. Report. https://cds.cern.ch/record/2696190

[20] M. Hofer, R. Tomás, Effect of local linear coupling on linear and nonlinear observables in circular accelerators. Phys. Rev. Accel. Beams. **23**(9), 094001 (2020). doi: 10.1103/PhysRevAccelBeams.23.094001

[21] D.D. Caussyn, M. Ball, B. Brabson et al., Experimental studies of nonlinear beam dynamics. Phys. Rev. A. **46**(12), 7942–7952 (1992). doi: 10.1103/PhysRevA.46.7942

[22] I. Hofmann, Space Charge Physics for Particle Accelerators (2017).

[23] A. Franchi, L. Farvacque, J. Chavanne et al., Vertical emittance reduction and preservation in electron storage rings via resonance driving terms correction. Phys. Rev. Spec. Top-AC. **14**, 034002 (2011). doi: 10.1103/PhysRevSTAB.14.034002

[24] E. Waagaard. Developing a resonance correction scheme in the LHC. CERN. Report. https://cds.cern.ch/record/2778017

[25] R.D. Maria, A. Latina, F. Schmidt, J. Dilly, Status of MAD-X V5.09. Paper presented at the 14th International Particle Accelerator Conference, Switzerland, May 2023. doi: 10.18429/JACoW-IPAC2023-WEPL101

[26] F. Schmidt, E. Forest, E. McIntosh, Introduction to the polymorphic tracking code: Fibre bundles, polymorphic Taylor types and "Exact tracking". CERN. Report. http://cds.cern.ch/record/573082

[27] K. Noda, T. Furukawa, S. Shibuya et al., Advanced RF-KO slow-extraction method for the reduction of spill ripple. Nucl. Instrum. Meth. A. **492**(1), 253–263 (2002). doi: 10.1016/S0168-9002(02)01319-0

[28] W.B. Ye, H.J. Yao, S.X. Zheng et al., Analysis and simulation of the tune ripple effect on beam spill ripple in RF-KO slow extraction. Nucl. Sci. Tech. **33**, 60 (2022). doi: 10.1007/s41365-022-01038-6

[29] S.Y. Lee, Accelerator physics (World Scientific Publishing Company, 2018)

[30] B.C. Jiang, Z.T. Zhao, S.Q. Tian et al., Using a double-frequency RF system to facilitate on-axis beam accumulation in a storage ring. Nucl. Instrum. Meth. A. **814**, 1–5 (2016). doi: 10.1016/j.nima.2016.01.024

[31] Z.B. Sun, L. Shang, F.L. Shang et al., Simulation study of longitudinal injection scheme for HALS with a higher harmonic cavity system. Nucl. Sci. Tech. **30**, 113 (2019). doi: 10.1007/s41365-019-0627-x

[32] X. Ming, D. Kang, Corrections for frequency, amplitude and phase in a fast fourier transform of a harmonic signal. Mech. Syst. Signal. Pr. **10**(2), 211–221(1996). 10.1006/mssp.1996.0015

[33] P. Odier, M. Ludwig, S. Thoulet, The DCCT for the LHC Beam Intensity Measurement. CERN. Report. https://cds.cern.ch/record/1183400

[34] R. Bartolini, F. Schmidt, Sussix: A Computer Code for Frequency Analysis of Non-Linear Betatron Motion. CERN. Report. https://cds.cern.ch/record/702438

[35] L. Wang, J.C. Yang, M.X. Chang et al., GOAT: a simulation code for high-intensity beams. Nucl. Sci. Tech. **34**, 78 (2023). doi: 10.1007/s41365-023-01225-z